Supporting Information

Simple air calcination affords commercial carbon cloth with high areal capacitance for symmetrical supercapacitors

Yi-Jie Gu [a], Wei Wen [a,b] and Jin-Ming Wu* [a]*

[a] State Key Laboratory of Silicon Materials and School of Materials Science and Engineering, Zhejiang University, Hangzhou 310027, P. R. China.

[b] College of Mechanical and Electrical Engineering, Hainan University, Haikou 570228, P. R. China.

Calculations of the areal specific capacitance and areal specific energy

The areal specific capacitance and areal specific energy are important indicators for evaluating flexible supercapacitor electrodes; the electrochemical tests in current investigation are therefore set according to the area ratio parameters.[1, 2] The areal specific capacitance of single electrode (C_{ele1}, C_{ele2}) was calculated from CV and GCD curves according to equations (1) and (2), respectively,[1-3]

$$C_{ele1}=\frac{\int I_1 \times \mathrm{d}V}{S \times v_1 \times \Delta V_1} \quad (1)$$

$$C_{ele2}=\frac{2\mathrm{I}_2 \times \Delta \mathrm{t}_2}{\Delta V_2} \quad (2)$$

In equation (1), S (1.131 cm^2) is the projected area of individual textile electrode, I_1 is the voltammetric current, v_1 is the scan rate, ΔV_1 is the potential window. In equation (2), I_2 is

the charge/discharge current density, Δt_2 is the discharge time, ΔV_2 is the potential window during the discharge process (excluding IR drop). Areal specific capacitance (C_{dev}), energy density (E_{dev}) and power density (P_{dev}) of the full-cell symmetric supercapacitor devices were calculated from GCD curves according to equations (3)-(5),[1, 2]

$$C_{\text{dev}} = \frac{\mathrm{I}_2 \times \Delta \mathrm{t}_2}{\Delta V_2} \tag{3}$$

$$E_{\text{dev}} = \frac{C_{\text{dev}} \times \Delta V_2^2}{2} \tag{4}$$

$$P_{\text{dev}} = \frac{E_{dev}}{\Delta t_2} \tag{5}$$

where I_2, ΔV_2 and Δt_2 have the same meanings as those in equation (2).

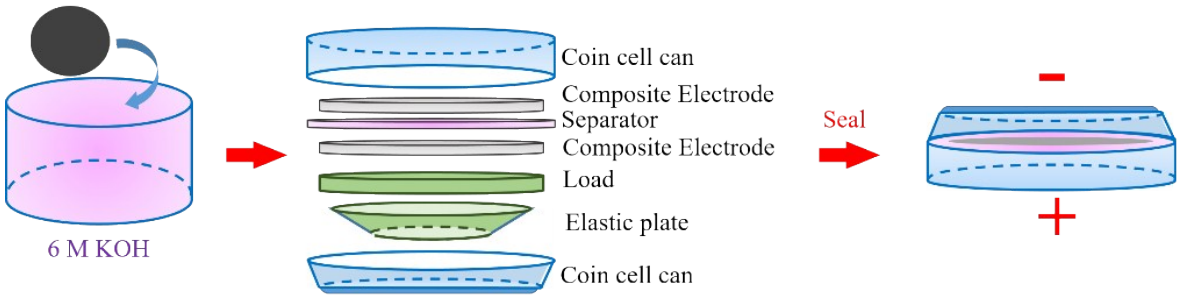

Figure S1. Assembly of full-cell supercapacitors.

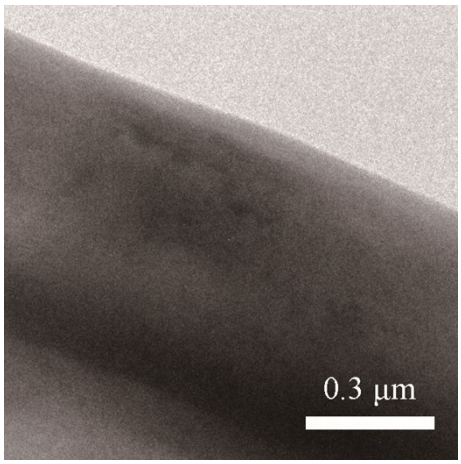

Figure S2. FESEM image of the pristine carbon cloth (UCC).

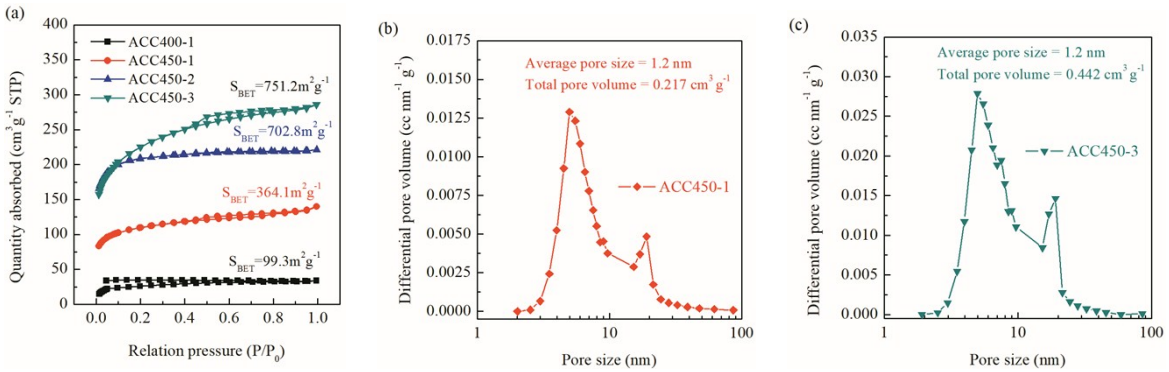

Figure S3. (a) Low-temperature N_2 adsorption/desorption isotherms of ACC400-1, ACC450-1, ACC450-2 and ACC450-3. Pore size distributions of ACC450-1 (b) and ACC450-3 (c), respectively.

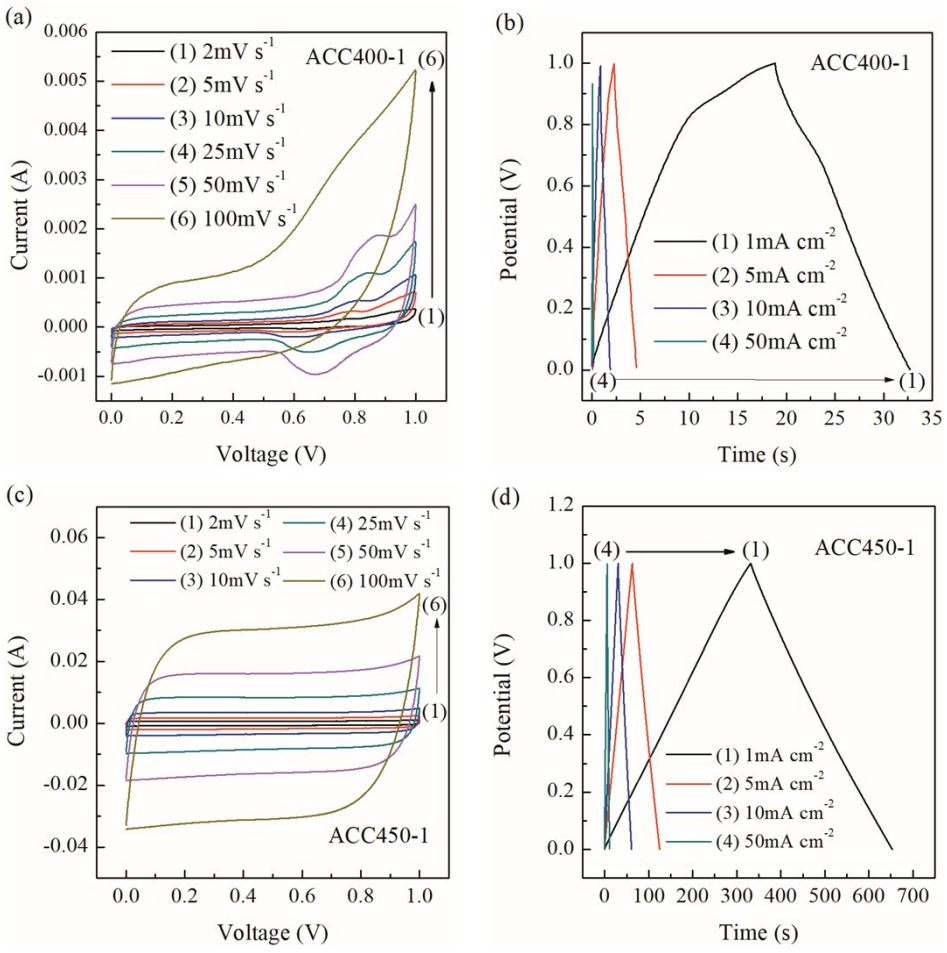

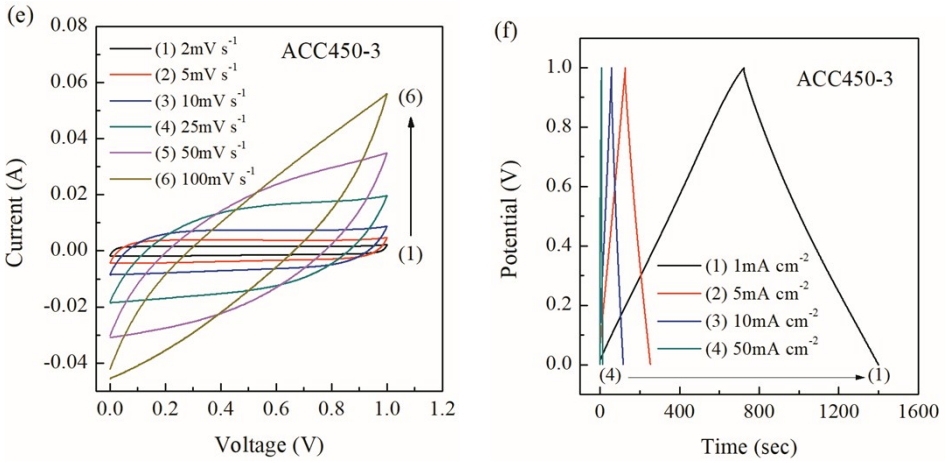

Figure S4. (a, c, e) CV curves and (b, d, f) GCD curves of ACC400-1, ACC450-1 and ACC450-3 at various scan rates from 2 to 100 mV s^{-1} and various current densities from 1 to 50 mA cm^{-2}, respectively.

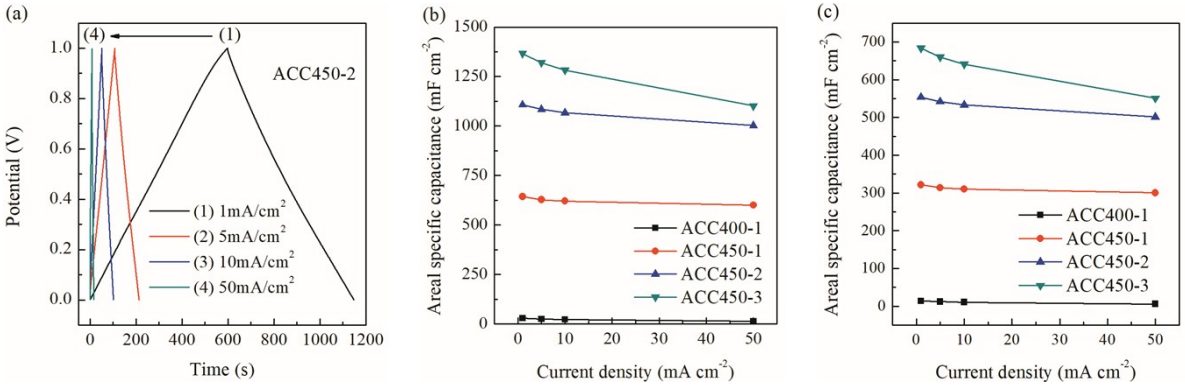

Figure S5. (a) GCD curves of ACC450-2 at various current densities ranging from 1 to 50 mA cm^{-2}. Areal capacitances of (b) the ACC electrodes and (c) the corresponding devices calculated from the GCD curves as a function of current density. Areal capacitance values of electrodes were calculated from GCD curves according to equation (2).

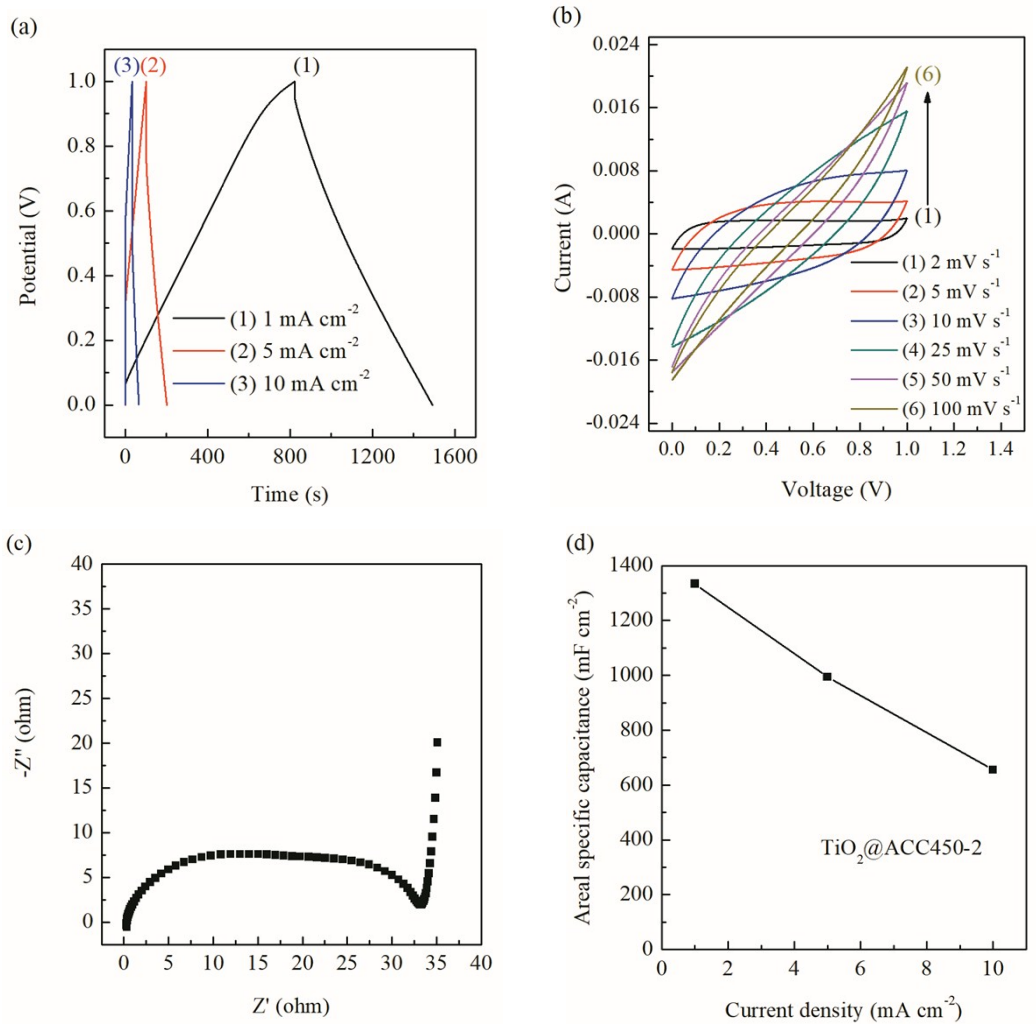

Figure S6. GCD curves (a) and CV curves (b) of TiO_2@ACC450-2 at various current densities ranging from 1 to 10 mA cm^{-2} and various scan rates from 2 to 100 mV s^{-1}, respectively. Comparative Nyquist plot (c) of electrochemical spectra of TiO_2@ACC450-2. Areal capacitances (d) of the TiO_2@ACC450-2 electrodes calculated from the GCD curves.

Fig. S6a shows GCD curves of TiO_2@ACC450-2 at various current densities ranging from 1 to 10 mA cm^{-2}. The TiO_2@ACC450-2 electrode exhibits symmetric and linear V-shaped charge-discharge curves, because of the fact that EDLCs dominantly contribute to the overall capacitance (Fig. S6a). Fig. S6b shows CV curves of TiO_2@ACC450-2 at various scan rates from 2 to 100 mV s^{-1}. The CV curves of TiO_2@ACC450-2 have a shuttle shape at high scan rate of 50 and 100 mV s^{-1}. The EIS test carried out at open circuit potential with an AC perturbation of 5 mV in the frequency range of 1000 kHz to 0.01 Hz. Fig. S6c shows the

Nyquist plot of the symmetric supercapacitors. The quasi-vertical profile of the sample TiO_2@ACC450-2 in the low-frequency region indicates that the device has nearly an ideal supercapacitor behavior. Additionally, the large diameter of the semicircle in the high-frequency region suggests a sluggish charge transfer process. Therefore, the areal specific capacitance is high (1333.8 mF cm^{-2}) at current density of 1 mA cm^{-2}; but decayed rapidly to 655 mF cm^{-2} upon the increasing current density to 10 mA cm^{-2}.

Table S1. Comparison of the volumetric capacitances of ACC electrodes and devices in this work and other carbon based materials reported in literatures.[4-10]

Material	C_v (for device or electrode) ($F\ cm^{-3}$)	Ref.
PANI-ZIF-67-CC	0.116 (for device)	4
MnO_2@TiN//EACC-10	2.69 (for device)	4
ACC	0.36 (for device)	5
Bamboo-like carbon nanofibers	2.1 (for device)	6
H-TiO_2@MnO_2//H-TiO_2@C	0.71 (for device)	7
TiN/carbon cloth	0.33 (for device)	8
PANI/MWCNT/PDMS	2.1 (for device)	9
CC	0.025 (for electrode)	10
OCC-15	0.5844 (for electrode)	10
ECC-15	15.8 (for electrode)	10
ACC450-1	**1.60 (for device), 10.67 (for electrode)**	**This work**
ACC450-2	**2.77 (for device), 18.47 (for electrode)**	**This work**
ACC450-3	**3.42 (for device), 22.8 (for electrode)**	**This work**
TiO_2@ACC450-1	**3.04 (for device), 20.27 (for electrode)**	**This work**
TiO_2@ACC450-2	**3.34 (for device), 22.27 (for electrode)**	**This work**

Abbreviations in Table S1

PANI: polyaniline; **CC:** carbon cloth; **ACC:** Activated carbon cloth; **EACC:** electrochemical activated carbon cloth; **H-**TiO_2: hydrogenated TiO_2; **MWCNT**: multi-wall carbon nanotube; **PDMS**: poly (dimethylsiloxane); **OCC:** oxide carbon cloth; **ECC:** electrochemical carbon cloth

Table S2. Comparison of the electrochemical performance of TiO_2@ACC450-2 in this work and other TiO_2 based materials reported in literatures.[11-25]

Material	Electrolyte	Capacitance	Ref.
TiO_2 NRs/FTO	1 M Na_2SO_4	85 μF cm^{-2} (5 mVs^{-1})	11
TiO_2 NRs/Ti foil	1 M Na_2SO_4	856.2 μF cm^{-2} (1 mVs^{-1})	12
TiO_2 NWs/Ti foil	0.5 M Na_2SO_4	121.5 mF cm^{-2} (1 mV s^{-1})	13
H-TiO_2-II phase NWs	0.5 M Na_2SO_4	710.7 mF cm^{-2} (1 mA cm^{-2})	14
H-TiO_2 NTAs/Ti fiber	0.5 M Na_2SO_4	3.24 mF cm^{-2} (100 mV s^{-1})	15
H-TiO_2 NTAs	2 M Li_2SO_4	7.22 mF cm^{-2} (0.05 mA cm^{-2})	16
TiO_2 NTAs	2 M Li_2SO_4	20.96 mF cm^{-2} (0.05 mA cm^{-2})	17
Nitridated hierarchical TiO_2 NTAs	0.5 M Na_2SO_4	85.7 mF cm^{-2} (10 mV s^{-1})	18
TiO_2@MnO_2 NTAs	0.5 M Na_2SO_4	150.9 mF cm^{-2} (0.5 A g^{-1})	19
TiO_2@C	0.5 M H_2SO_4	210 F g^{-1} (0.2 A g^{-1})	20
Ti@CNFs	6 M KOH	280 F g^{-1} (1 A g^{-1})	21
PPy/SWCNT/TiO_2	1 M KCl	281.9 F g^{-1} (0.5 A g^{-1})	22
Graphene–TiO_2	1 M Na_2SO_4	165 F g^{-1} (5 mVs^{-1})	23
TiO_2/CNT	1 M KOH	135 F g^{-1}	24

		(1 A g^{-1})	
H-TiO_2@C	5 M LiCl	253.4 F g^{-1} (10 mV s^{-1})	7
H-TiO_2@MnO_2	5 M LiCl	449.6 F g^{-1} (10 mV s^{-1})	
TiO_2/MnO_2-C core/shell arrays	1 M Na_2SO_4	630 F g^{-1} (5 A g^{-1})	25
ACC450-2	**6 M KOH**	**1137 mF cm^{-2}** (81.2 F g^{-1} calculated based on the single electrode total mass, 2 mV s^{-1})	**This work**
TiO_2@ACC450-1	**6 M KOH**	**1216 mF cm^{-2}** (901 F g^{-1} calculated based on the mass of active material TiO_2, 2 mV s^{-1})	**This work**

Abbreviations in Table S2

NRs: nanorods; **NWs**: nanowires; **NTAs**: nanotube arrays; **CNT**: carbon nanotube; **SWCNT**: single-wall carbon nanotube; **PPy**: polypyrrole; **H**-TiO_2: hydrogenated TiO_2

REFERENCES

1. L. Dong, C. Xu, Q. Yang, J. Fang, Y. Li, F. Kang, J. Mater. Chem. A, 2015, 3, 4729.
2. M. Stoller, R. Ruoff, Energy Environ. Sci., 2010, 3, 1294.
3. C. Hsieh, H. Teng, Carbon, 2002, 40, 667.
4. W. Wang, W. Liu, Y. Zeng, Y. Han, M. Yu, X. Lu and Y. Tong, Adv. Mater., 2015, 27, 3572.
5. G. Wang, H. Wang, X. Lu, Y. Ling, M. Yu, T. Zhai, Y. Tong, Y. Li, Adv. Mater., 2014, 26, 2676.
6. Y. Sun, R. B. Sills, X. Hu, Z. W. Seh, X. Xiao, H. Xu, W. Luo, H. Jin, Y. Xin, T. Li, Z. Zhang, J. Zhou, W. Cai, Y. Huang, Y. Cui, Nano Lett., 2015, 15, 3899.
7. X. Lu, M. Yu, G. Wang, T. Zhai, S. Xie, Y. Ling, Y. Tong, Y. Li, Adv. Mater., 2013, 25, 267-272.
8. X. Lu, G. Wang, T. Zhai, M. Yu, S. Xie, Y. Ling, C. Liang, Y. Tong, Y. Li, Nano Lett., 2012, 12, 5376.

9. M. Yu, Y. Zhang, Y. Zeng, M. S. Balogun, K. Mai, Z. Zhang, X. Lu and Y. Tong, Adv. Mater., 2014, 26, 4724.

10. D. Ye, Y. Yu, J. Tang, L. Liu, Y. Wu, Nanoscale, 2016, 8, 10406.

11. A. Ramadoss, S. Kim, J. Alloy. Compd., 2013, 561, 262.

12. Z. Zheng, J. Chen, R. Yoshida, X. Gao, K. Tarr, Y. Ikuhara, W. Zhou, Nanotechnology, 2014, 25, 435406.

13. W. Guo, Y. Li, Y. Tang, S. Chen, Z. Liu, L. Wang, Y. Zhao, F. Gao, Electrochim. Acta, 2017, 229, 197.

14. Y. Tang, Y. Li, W. Guo, J. Wang, X. Li, S. Chen, S. Mu, Y. Zhao, F. Gao, J. Mater. Chem. A, 2018, 6, 623.

15. X. Lu, G. Wang, T. Zhai, M. Yu, J. Gan, Y. Tong, Y. Li, Nano lett., 2012, 12, 1690.

16. H. Wu, C. Xu, J. Xu, L. Lu, Z. Fan, X. Chen, Y. Song, D. Li, Nanotechnology, 2013, 24, 455401.

17. C. Zhang, J. Xing, H. Fan, W. Zhang, M. Liao, Y. Song, J Mater Sci., 2017, 52, 3146.

18. N. Nguyen, S. Ozkan, I. Hwang, X. Zhou, P. Schmuki, J. Mater. Chem. A, 2017, 5, 1895.

19. H. Zhou, X. Zou, Y. Zhang, Electrochim. Acta, 2016, 192, 259.

20. L. Hou, H. Hua, H. Cao, S. Zhu, C. Yuan, RSC Adv., 2015, 5, 62424.

21. K. Tang, Y. Li, H. Cao, C. Su, Z. Zhang, Y. Zhang, Electrochim. Acta, 2016, 190, 678.

22. A. Oliveira, H. Oliveira, J. Power Sources, 2014, 268, 45.

23. A. Ramadoss, S. Kim, Carbon, 2013, 63, 434.

24. X. Sun, M. Xie, J. Travis, G. Wang, H. Sun, J. Lian, S. George, J. Phys. Chem. C, 2013, 117, 22497.

25. Q. Xiong, C. Zheng, H. Chi, J. Zhang, Z. Ji, Nanotechnology, 2017, 28, 55405.